J. Space Weather Space Clim. 2024, **14**, 24

https://doi.org/10.1051/swsc/2024023

JSWSC

Available online at:
www.swsc-journal.org

RESEARCH ARTICLE OPEN ACCESS

Long-term relationships of ionospheric electron density with solar activity

Norbert Jakowski[1,*], Mohammed Mainul Hoque[1], and Jens Mielich[2]

[1] German Aerospace Center, Institute for Solar-Terrestrial Physics, Kalkhorstweg 53, 17235 Neustrelitz, Germany
[2] Leibniz Institute of Atmospheric Physics, Schloßstraße 6, 18225 Kühlungsborn, Germany

Received 19 January 2024 / Accepted 21 June 2024

Abstract – Greenhouse gases such as carbon dioxide and methane that are causing climate change may cause long-term trends in the thermosphere and ionosphere. The paper aims to contribute to exploring long-term effects in the ionosphere focusing on the impact of solar activity changes. Peak electron density data derived from vertical sounding measurements covering 65 years at the ionosonde stations Juliusruh (JR055), Boulder (BC840), and Kokubunji (TO536), have been utilized to estimate the long-term behavior of daytime ionospheric F2 layer ionization in relation to the solar 10.7 cm radio flux index F10.7. In parallel, Global Navigation Satellite System (GNSS) based vertical total electron content (TEC) data over the ionosonde stations in combination with the peak electron density data have been used to derive the equivalent slab thickness τ for estimating long-term behavior in the period 1996–2022. A new approach has been developed for deriving production and loss term proxies for studying long-term ionization effects from F2 layer peak electron density and TEC data. The derived coefficients allow for estimating the long-term variation of atomic oxygen and molecular nitrogen concentrations including their ratio during winter months. The noon-time slab thickness values over Juliusruh correlate well with the decrease of F10.7 and the F2 layer peak height and enable estimating the neutral gas temperature. The equivalent slab thickness decreases by about 20 km per decade in the period 1996–2022, indicating a thermospheric cooling of about 100 K per decade for Juliusruh. Whereas the oxygen concentration decreases, the loss term, considered as a proxy for molecular components of the neutral gas, in particular N_2, increases with the long-term solar activity variation. Considering 11-year averages of the production and loss terms under wintertime conditions, the long-term study reveals for the O/N_2 ratio a percentage decrease of 5% per decade and for F10.7 about 3.1% per decade in a linear approach referred to the year 1970. Linear models of 11 years averaged NmF2 and foF2 from corresponding F10.7 show a very close correlation with the temporal variation of F10.7 until about 1990. The root mean square errors are in the order of 1.0–1.3 · 10^{10} m^{-3} for NmF2 and 0.03–0.05 MHz for foF2. After 1990 the linear models deviate from F10.7 at all selected mid-latitude ionosonde stations indicating a non-local effect.

Keywords: Ionosphere / Vertical sounding / Equivalent slab thickness / Solar activity / Long-term trends

1 Introduction

Earth's atmosphere is experiencing long-term changes due to the increasing concentration of carbon dioxide and other trace gases. Thus, the question arises as to how climate change, observable at the Earth's troposphere and hydrosphere, impacts the Geo-space in the thermosphere and ionosphere and how significant such changes are.

Long-term trends of atmospheric and ionospheric behavior have been studied for more than 3 decades starting with modeling of consequences of an increased concentration of carbon dioxide and methane by Roble & Dickinson (1989). Considering these results in light of the basic theory of the ionosphere, Rishbeth (1990) concluded that the predicted so-called "global cooling" of the thermosphere would not have significant consequences for the electron density. The main ionospheric consequences could appear as a decrease of the F2 layer peak height hmF2 by about 15-20 km. This conclusion is underlined by Solomon et al. (2015) by 3D simulation studies. On the other hand, assuming doubled CO_2, simulation studies by Qian et al. 2009 running a coupled thermosphere and ionosphere general circulation model revealed a significant reduction of the peak density height hmF2 and peak density NmF2 of up to 40% depending on diverse geophysical factors like geographic

*Corresponding author: norbert.jakowski@dlr.de

location, local time, season and solar activity level. Considering these different estimations, further studies are needed utilizing new data sets.

Considering the availability of long-term observations by ionosonde stations, many attempts have been made to derive long-term trends of ionospheric parameters such as foF2, hmF2 or foE (Bremer, 1992; Rishbeth, 1997; Mikhailov & Marin, 2001; Hall et al., 2011; Laštovička et al., 2006; Bremer et al., 2012; Mielich & Bremer, 2013; Cnossen & Franzke, 2014; Sivakandan et al., 2023). A comparison of different methods for deriving foF2 long-term trends is given by Laštovička et al. (2006). Considering highly reliable Juliusruh foF2 data within the years 1976–1996, they found either very small negative or insignificant trends. Weak or even ambiguous results are obtained also in other studies (e.g. Ulich et al., 2003; Laštovička et al., 2012; Cai et al., 2019).

Due to the complex coupling processes in the magnetosphere-ionosphere-thermosphere (MIT) system, many processes are modified if only one parameter is changing. Related problems have been addressed by Danilov (2017) and Laštovička & Jelínek (2019). Whereas Danilov (2017) underlines the impact of data length and seasonal and diurnal effects, Laštovička & Jelínek (2019) consider natural variability, data problems, and methodology separately. Some methodology uncertainties may be introduced by considering the entire day, allowing all seasons to be included, and not specifying the period and length of the initial data series as pointed out by Danilov (2017). Furthermore, besides the main solar activity control and changes (Tapping & Valdés 2011) several impact factors have the potential to substantially modify the ionospheric electron density due to complex mechanisms of action. These are for example: long-term changes in geomagnetic field configuration that can affect the electron density via changes in plasma transport and via changes in the geographic distribution of energetic particle precipitation at high-latitudes (e.g. Cnossen & Richmond 2008, 2013; Elias et al., 2010). Variations in geomagnetic activity levels affect also in particular the high latitude ionosphere via changes in energetic particle precipitation (Mikhailov & Marin, 2001; Cnossen & Franzke, 2014). Changes in the concentration of atomic oxygen and molecular nitrogen affect the production and loss processes (Zhang & Paxton, 2011; Danilov, 2017; Perrone et al., 2017). Changes in dynamic coupling processes from below e.g. gravity waves can cause cooling in the thermosphere and changes in turbulent mixing and related effects are not yet well understood (Oliver et al., 2013). Finally, changes in the greenhouse gas concentration may also affect the temperature and structure of the ionosphere (Qian et al., 2006, 2009; Solomon et al., 2015). Thus, separating a potential anthropogenic impact on ionospheric observables from their natural variability is an extremely difficult task.

As underlined by Laštovička & Jelínek (2019), a long-time series of consistent and homogeneous measurements are required to be suitable for trend studies.

With the permanent availability of GPS signals since 1995, additional parameters such as the Total Electron Content (TEC) and the equivalent slab thickness, commonly abbreviated by τ, have been used for long-term studies (Lean et al., 2016; Emmert et al., 2010, 2017; Laštovička et al., 2017; Jakowski et al., 2017; Zhang et al., 2021). Following the classical Chapman theory, the equivalent slab thickness τ, defined by τ = TEC/NmF2, is proportional to the thermospheric scale height under diffusive equilibrium conditions. Since the thermospheric scale height is proportional to the neutral gas temperature T_n, the equivalent slab thickness is directly related to the neutral gas temperature. Because NmF2 corresponds to the F2 layer peak height hmF2 and the center of mass of TEC refers to an altitude range of about 350–400 km, it is expected that the equivalent slab thickness has the potential to estimate the neutral gas temperature in the topside ionosphere under diffusive equilibrium conditions in the ionosphere around noon. Thus, thermospheric cooling could be studied by analyzing noontime equivalent slab thickness data (Jakowski et al., 2017). Being aware that solar irradiation dominates the long-term electron density behavior, identification of changes in the relationship between solar activity and ionospheric variables over a long time can help to clarify the underlying physical mechanism in long-term trends. Hence, we compare the long-term variation of the solar radio flux index F10.7 with the variation of ionospheric variables like NmF2, foF2, and TEC using a linear approach to check whether the relationship is conserved or changes over time. In Section 3.1 we focus the analysis on the period 1996–2022 which enables us to study the long-term behavior of TEC and the equivalent slab thickness over more than two solar cycles. For the first time, we consider the long-term behavior of production and loss coefficients of balance equations for NmF2 and TEC. The results should help to better understand and get some ideas for modeling the long-term variation of the electron density in relation to solar activity changes. Following this idea, we have modeled the variation of NmF2 and foF2 to derive long-term trends of these parameters described in chapter 3.4. For this modeling approach, we have used long-term ionosonde foF2 data covering more than five solar cycles from three ionosonde stations Juliusruh (54.6°N; 13.4°E), Kokubunji (35.7°N; 139.5°E) and Boulder (41.6°N; 254.7°E) and related TEC including equivalent slab thickness observations since 1996, thus covering more than two solar cycles.

2 Database and data preparation

The peak electron density NmF2 and peak electron density height hmF2 used in this study are derived from ground-based vertical sounding observations recorded in so-called ionograms. In this paper, we use manually scaled data of critical frequencies foF2 and derived hmF2 from the ionosonde station Juliusruh (JR055) which has been continuously operating since 1957 over more than 5 solar cycles. The data are obtained directly from the Juliusruh observatory, but can also be obtained from the ionospheric section of the WDC at the Australian Space Weather Forecasting Centre https://www.sws.bom.gov.au/World_Data_Centre/1/3. The F2 peak density height hmF2 is calculated using the so-called propagation factor M(3000)F2 (M(3000)F2=MUF(3000)F"/foF2) obtained from manually scaled M(3000)F2 values derived from ionograms and the formula given by Shimazaki (1955):

$$\mathrm{hmF2} = 1490/\mathrm{M(3000)F2} - 176. \quad (1)$$

Manually scaled foF2 data from the Japanese station Kokubunji (TO535/TO536) are obtained from the National Institute of

Table 1. Coordinates and data coverage of vertical sounding stations used in the paper.

Ionosonde station	URSI ID	Geographic latitude [°N]	Geographic longitude [°E]	foF2/NmF2 data coverage
Juliusruh	JR055	54.6	13.4	1958–2022
Kokubunji	TO536	35.7	139.5	1958–2022
Boulder	BC840	41.6	254.7	1958–2002 2004–2022

Information and Communications Technology https://wdc.nict.go.jp/IONO/HP2009/ISDJ/index-E.html.

foF2 data from the US-station Boulder (BC840) are obtained from World Data Center C1 https://www.ukssdc.ac.uk/cgi-bin/wdcc1/secure/iono_data.pl (1958/07–2002/12, manually scaled) and from the Global Ionospheric Radio Observatory (Reinisch & Galkin, 2011) https://giro.uml.edu/didbportal/didb-web-portal/ (2004/03–2022/12, automatically scaled).

The peak electron density NmF2 analyzed and required for computing the equivalent slab thickness is derived from foF2 vertical sounding data by the relation

$$\mathrm{NmF2} = 1.24 \cdot 10^{-2}(\mathrm{foF2})^2 \qquad (2)$$

in SI units.

An overview of ionosonde stations used in this study is given in Table 1.

The accuracy of foF2 estimates is in the order of 0.1 MHz (about $2 \cdot 10^{10}$ m^{-3} at 9 MHz) for manually scaled values from undisturbed ionograms or less than 0.5 MHz for automatically scaled ionograms. From all stations half-hourly data sets of foF2 (1958–2022) have been prepared for each day, hmF2 data (1996–2022) only from Juliusruh. Since we need at least a half-hourly time resolution in subsequent data analysis, original hourly data have been linearly interpolated. To reject outliers, which commonly appear in observation data, we have extracted monthly medians for further analysis. If needed and if no more than one value is missing in the time series, we have filled data gaps by linear interpolation between neighbor values, e.g. missing yearly averaged noontime data at BC840 in 2003 have been interpolated by using corresponding data from 2002 to 2004. The median foF2 data have then been transformed into electron density values according to equation (2). Furthermore, we have calculated central time derivatives spanning a time interval of 1 h for each half hour.

TEC data are commonly derived from radio signals of Global Navigation Satellite Systems (GNSS) at two coherent L band frequencies. The analysis procedure of how TEC data can be derived from GNSS measurements is described in former publications (e.g. Jakowski, 1996; Jakowski et al., 2011). For computing the equivalent slab thickness τ over vertical sounding stations the related vertical TEC data are converted from measured slant radio link-related TEC measurements as described by Jakowski et al. (2017). TEC data over JR055 were provided by DLR (SWACI – Space Weather Application Center Ionosphere project) up to 2010 (Jakowski et al., 2008). SWACI TEC data having a time resolution of 10 min were limited over the European region and available from 1995 until 2010. Therefore, we could use SWACI data only for the Juliusruh station until 2010. Later, TEC data provided by the International GNSS Reference Service (IGS) were used. Thus, CODE (Center for Orbit Determination in Europe) is an IGS associate analysis center and has been routinely generating a Global Ionosphere Map (GIM) daily since 1996 (Schaer et al., 1998). Daily IONEX (IONosphere EXchange) files of one/two hourly (one-hour resolution since 2015) global TEC maps were downloaded from the CDDIS (Crustal Dynamics Data Information System; Noll, 2010) archive ftp://cddis.gsfc.nasa.gov/pub/gps/products/ionex. TEC values were interpolated over ionosonde stations every half an hour using spatial and temporal interpolation. Note that for Kokubunji and Boulder stations only CODE TEC data were used since SWACI data only covers the European region.

The derived half-hourly vertical TEC data sets (1996–2022) over the selected ionosonde stations have been combined with half-hourly NmF2 and hmF2 data. Finally, central time derivates were computed for each half hour and then monthly medians were computed. For correlating the ionosphere data with the solar activity level, we used the well-known solar radio flux index at 10.7 cm wavelength (F10.7). For longer time scales F10.7 is the most suitable index as shown by Wintoft (2011) and confirmed in ionospheric studies by Mielich & Bremer (2013). Monthly averaged values of F10.7 are available via the NOAA archive: https://www.ngdc.noaa.gov/stp/space-weather/solar-data/solar-features/solar-radio/noontime-flux/penticton/penticton_absolute/listings/listing_drao_noontime-flux-absolute_monthly.txt, since 1947. The daily measured solar radio flux or Penticton index F10.7 has been made by the National Research Council of Canada (NRCC) since 1947 and is measured in so-called solar flux units (1 sfu = 10^{-22} W Hz^{-1}m^{-2}).

3 Observations and discussion

As already mentioned, two time periods will be considered in this paper. Thanks to long-term foF2 data sets from ionosonde stations Juliusruh, Boulder, and Kokubunji, covering more than 65 years from 1958 to 2022, there is a possibility to estimate reliable long-term changes in relation to the solar activity given by the solar radio flux index F10.7. The other key parameter of the ionosphere, the TEC, is continuously available after GPS became operational in 1995. Thus, starting with complete data sets for Juliusruh in 1996, we were able to study the temporal variation of TEC and the equivalent slab thickness over 2½ solar cycles. To reduce the impact of diurnal dynamics we focus in the subsequent analysis on nearly equilibrium conditions in the ionosphere and selected data. Following this strategy, we selected our study for all parameter values around noon, including the period 12–14 LT, being aware that the peak density is commonly reached after 12 LT. Thus, if

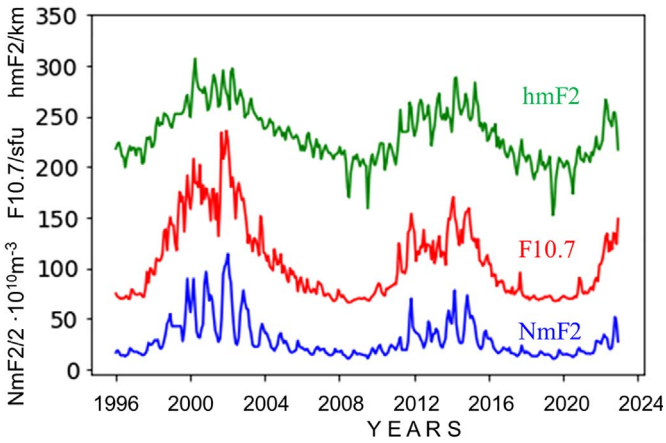

Figure 1. Solar cycle dependence of monthly noontime medians of ionosonde parameters NmF2 and hmF2 over Juliusruh compared with the solar activity proxy F10.7 for solar cycles 23–25.

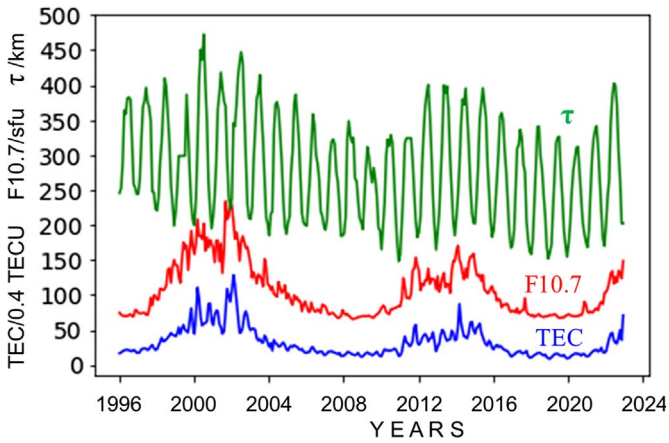

Figure 2. Solar cycle dependence of monthly noontime medians of ground-based TEC measurements and τ over Juliusruh in comparison with the solar activity proxy F10.7 for solar cycles 23–25.

not explicitly mentioned otherwise, the presented results refer always to mid-day conditions around 13 LT.

3.1 Long-term TEC and equivalent slab thickness behavior

To get a general impression of the variability of analyzed ionospheric key parameters, Figure 1 shows the variation of monthly medians of the F2 layer peak electron density NmF2 and peak height hmF2 at noon in the years 1996–2022 over Juliusruh in comparison with related monthly means of F10.7. Whereas the minimum values of F10.7 are relatively stable, the peak values around the years 2012–2015 are substantially lower compared with the maximum around 2000–2003. The related peak electron density NmF2 and the peak height hmF2 behave similarly as the subsequent analysis will show in more detail.

Similar plots for vertical TEC and the equivalent slab thickness are shown in Figure 2. The equivalent slab thickness τ is computed by the relationship:

$$\tau = \frac{\mathrm{TEC}}{\mathrm{NmF2}}. \tag{3}$$

Again, the data indicate a clear seasonal variation superposed on a long-term decrease associated with the decreasing solar activity index F10.7. For studying the long-term trend in more detail, the strong seasonal variation of NmF2, hmF2, TEC, and τ is removed by computing yearly averages. Since the availability of full yearly TEC data sets started in 1996 at the earliest, the subsequent data analysis for stations Juliusruh, Kokubunji and Boulder considers the time window 1996–2022 covering $2^1/_2$ solar cycles.

The variation of yearly averages of noontime TEC over all three stations is shown in Figure 3 in comparison with corresponding linear regression lines. Availability of reliable TEC data at Boulder and Kokubunji start somewhat later, in 2000 and 2002, respectively.

The negative slopes per decade derived for all parameters from related linear regression lines are summarized in Table 2. The associated Pearson correlation coefficients of parameters with F10.7 and the Root Mean Square Errors (RMSE) are also provided in Table 2.

A comparison of the temporal variation of the equivalent slab thickness at all three stations is shown in Figure 4. Considering the similar behavior of τ over the stations it is worth mentioning that the derived slopes of the regression lines are somewhat different. This is obviously due to the different start times of data intervals: JR055 in 1996, BC840 in 2000, and TO536 atin 2002 resulting accordingly in quite different slopes for F10.7 (Table 2). It is confirmed that derived slopes depend considerably on the years analyzed and the interval length. The strong drop of the equivalent slab thickness over Juliusruh from 1996 to 2010 easily explains the rather high negative slope of −52 km/decade for τ reported in the earlier study by Jakowski et al. (2017). The longer time scale from 1996 to 2022 provides a much lower decrease of 25.6 km per decade which sounds more reasonable. This discrepancy underlines our understanding that reliable long-term studies require a time series covering at least more than two solar cycles.

Whereas the equivalent slab thickness over Juliusruh and Kokubunji behaves very similarly, the equivalent slab thickness over Boulder is about 20–40 km larger over the entire period of 20 years from 2002–2022. This fact remains unexplained but might be related to longitudinal effects and/or uncertainties in TEC data biases.

To reduce the solar activity impact Jakowski et al. (2017) proposed analyzing the equivalent slab thickness of the ionosphere because this quantity is less sensitive to the solar activity cycle and furthermore, is related to the neutral gas temperature under ionospheric equilibrium conditions around noon. To estimate the neutral gas temperature at peak electron density height we follow estimations made by Titheridge (1973). In his study, Faraday rotation measurements of TEC revealed an estimation of the thermospheric temperature T_n at peak density heights for daytime conditions according to:

$$T_n \approx (\tau - 15)/0.225. \tag{4}$$

Since Faraday rotation-based TEC estimates are more weighted at lower heights due to the decrease of the geomagnetic field

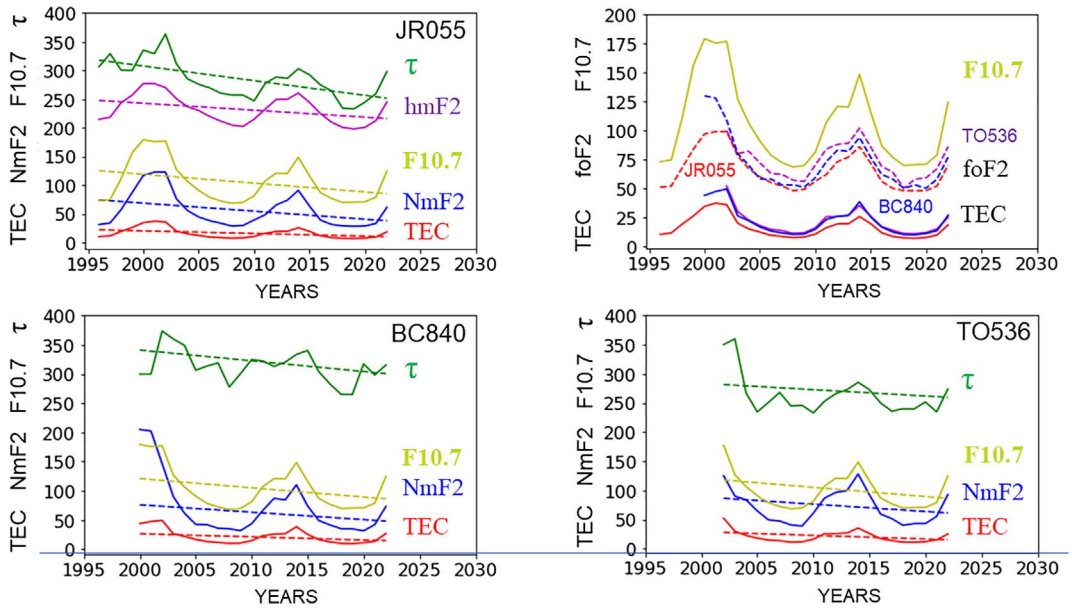

Figure 3. Yearly averages of TEC [TECU], NmF2 [10^{10} m^{-3}], foF2 [0.1 MHz], τ [km] and hmF2 [km] at noon in comparison with the solar F10.7 index [sfu] for selected ionosonde stations in the years 1996–2022 for Juliusruh, 2000–2022 for Boulder (2003 interpolated) and 2002–2022 for Kokubunji. Corresponding linear regression lines are dashed. The right upper panel shows the relationship between observed TEC, foF2, and F10.7.

Table 2. Linear regression line related decrease of ionospheric key parameters as slope per decade, Pearson correlation *R* with F10.7, and Root Mean Square Errors (RMSE) derived from data sets within the period 1996–2022.

Ionosonde station	Parameter	NmF2 [10^{10} m^{-3}]	foF2 [MHz]	TEC [TECU]	τ [km]	hmF2 [km]	F10.7 [sfu]
JR055 1996–2022	*R*	0.95	0.99	0.96	0.76	0.94	
	Slope	−14.0	−0.7	−4.6	−25.6	−12.1	−17.4
	RMSE	27.4	1.5	8.1	24.5	22.0	38.5
BC840 2000–2022	*R*	0.95	0.98	0.99	0.49		
	Slope	−41.1	−1.8	−9.0	−15.9		−26.9
	RMSE	46.5	1.96	10.9	25.7		32.0
TO536 2002–2022	*R*	0.97	0.95	0.98	0.79		
	Slope	−10.0	−0.5	−5.8	−25.7		−13.7
	RMSE	26.9	1.4	9.3	31.7		28.4

intensity with height, GNSS-based TEC data and related slab thickness estimates provide always higher values because they include the plasmasphere content (cf. Jakowski & Hoque, 2018). Being aware of this difference, we have modified the formula for GNSS-based estimates of the equivalent slab thickness according to:

$$T_n \approx (\tau - 40)/0.25 \quad (5)$$

with τ in km and T_n in K.

The obtained variation of T_n over Juliusruh during the period 1996–2022 is shown in Figure 5 in comparison with hmF2 and F10.7 variations. This estimation fits in a qualitative manner with results published by Zhang & Paxton (2011) who obtained an exospheric temperature decrease from about 1100–1500 K in 2003 to about 600–900 K in mid-2007 (see marked area in Fig. 5). In our estimation (cf. eq. (5) and Fig. 5) T_n decreases from about 1200 to 850 K in the same period. These values are consistent with temperatures modeled by Qian et al. (2006) decreasing from about 1250 to 700 K within the period from 2002 to 2005.

The high correlation of T_n and hmF2 with the solar activity index is expected. Enhanced solar energy input heats and expands the thermosphere leading to an enhanced peak height and enhanced scale heights resulting in an increased equivalent slab thickness. The derived average temperature decreases along the regression lines range from about 60–100 K per decade for selected stations. These values are higher than those obtained by simulation studies. Solomon et al. (2010) derived a decrease of 41 K at 400 km height with the NCAR Thermosphere-Ionosphere-Electrodynamics General Circulation Model for the time period 1996–2008 including realistic CO_2 changes. Cooling rates of more than 10 K/decade have been reported by Ogawa et al. (2014) after analyzing incoherent scatter measurements at EISCAT. Model runs by Solomon et al. (2015) under solar minimum conditions, assuming two different enhanced CO_2 levels in the thermosphere, have revealed temperature changes

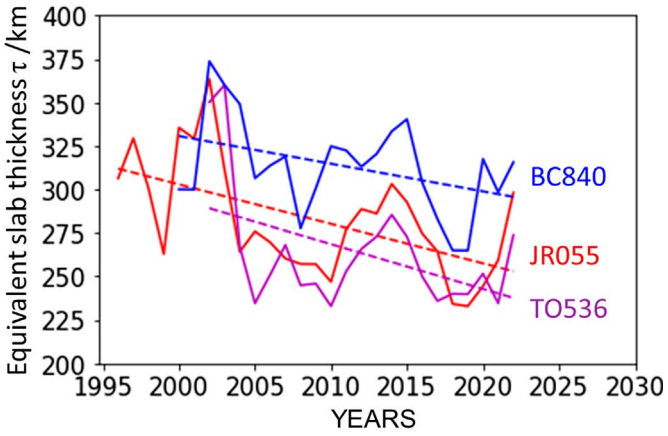

Figure 4. Variation of the equivalent slab thickness τ at local noon during the years 1996–2022 and corresponding linear regression lines (dashed). Start times for JR055: 1996, for BC840: 2000, for TO536: 2002

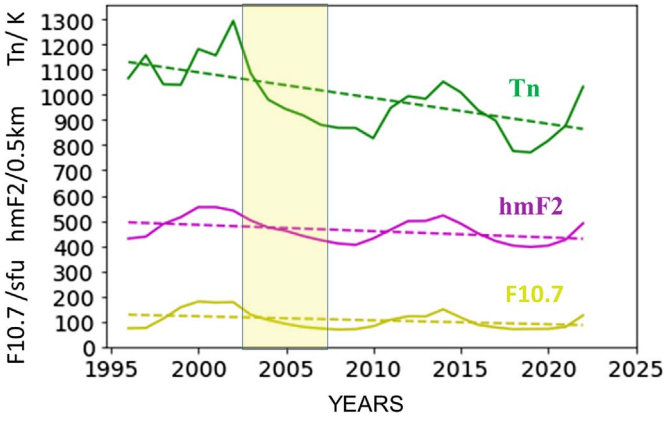

Figure 5. Estimation of the neutral gas temperature T_n [K] above the ionospheric peak height in comparison with hmF2 [0.5 km] estimates for Juliusruh and F10.7 [sfu] radio flux data. T_n slope: −102 K / decade; Pearson correlation coefficients R of T_n and hmF2 with F10.7: R = 0.76 and R = 0.94, respectively.

in the order of 2–5 K. Thus, following equation (5), the expected change of the equivalent slab thickness would be in the order of about 1–3 km. Considering the high variability of τ, a potential CO_2 impact is extremely difficult to detect via estimates of the equivalent slab thickness within one or two decades.

3.2 Long term foF2 and NmF2 behavior

To investigate the long-term behavior of ionospheric electron density in relation to the solar radiation input in more detail, very long-term data sets obtained at the selected ionosonde stations over 65 years are utilized. Data gaps occur in the observations over this very long-time span. This problem is reduced when analyzing data averaged over one year or solar cycle length. Those data have no gaps but one must be aware that the quality of averages might be impacted, e.g. if some months

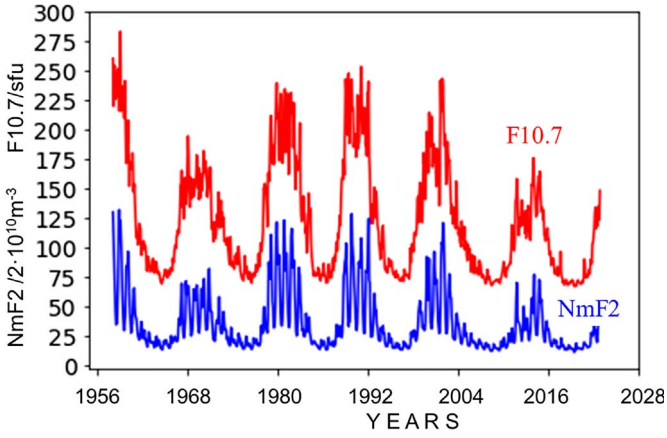

Figure 6. Long-term behavior of noontime NmF2 over Juliusruh in comparison with the solar radio flux index F10.7.

are missing when yearly averages are computed. The higher the degree of averaging, the smaller the effect of data gaps. Juliusruh provides nearly a complete foF2 data set from 01/01/1958 to 12/31/2022, thus guaranteeing a high quality of derived results.

As seen in Figure 6, the monthly medians of peak electron density (NmF2) of the F2 layer over Juliusruh show a high seasonal dynamic that follows the general behavior of the solar activity level over nearly six solar cycles. The relationship of NmF2 with the solar activity presented by the 10.7 cm radio flux will be studied in more detail in the subsequent chapter.

Figure 7 indicates a high correlation between yearly averages of NmF2 and F10.7. Performing a linear regression as made in the previous chapter is less attractive here due to the big variation of F10.7 indicating a maximum around 1990. Nevertheless, to get some insight into the long-term behavior, the data were averaged over an assumed mean solar cycle length of 11 years. The results, shown in Figure 7 (upper right panel) indicate a very similar long-term behavior of NmF2 values at all three ionosonde stations with F10.7. The Pearson correlation coefficient for the entire period 1970–2022 is R = 0.98 for all stations as carried out in more detail in the subsequent chapter. The temporal variation of NmF2 is very similar at all stations and the absolute levels of peak electron density correlate reasonably with the latitude of stations, i.e. they increase towards lower latitudes due to enhanced solar radiation input.

3.3 Long-term behavior of production and loss coefficients

All long-term variations seen in the results as presented in the previous chapter for various key parameters of the ionosphere are closely correlated with the solar activity characterized by the solar radio flux at 10.7 cm wavelength. Separating secondary effects from this dominant relationship requires an extremely careful analysis of observation data over long periods.

To investigate the cause of negative trends of ionospheric key parameters in more detail, the atmospheric composition, in particular atomic oxygen O and molecular nitrogen N_2 concentrations must be considered because their ratio has a strong impact on the ionization level (e.g. Torr et al., 1980; Jakowski et al., 2017).

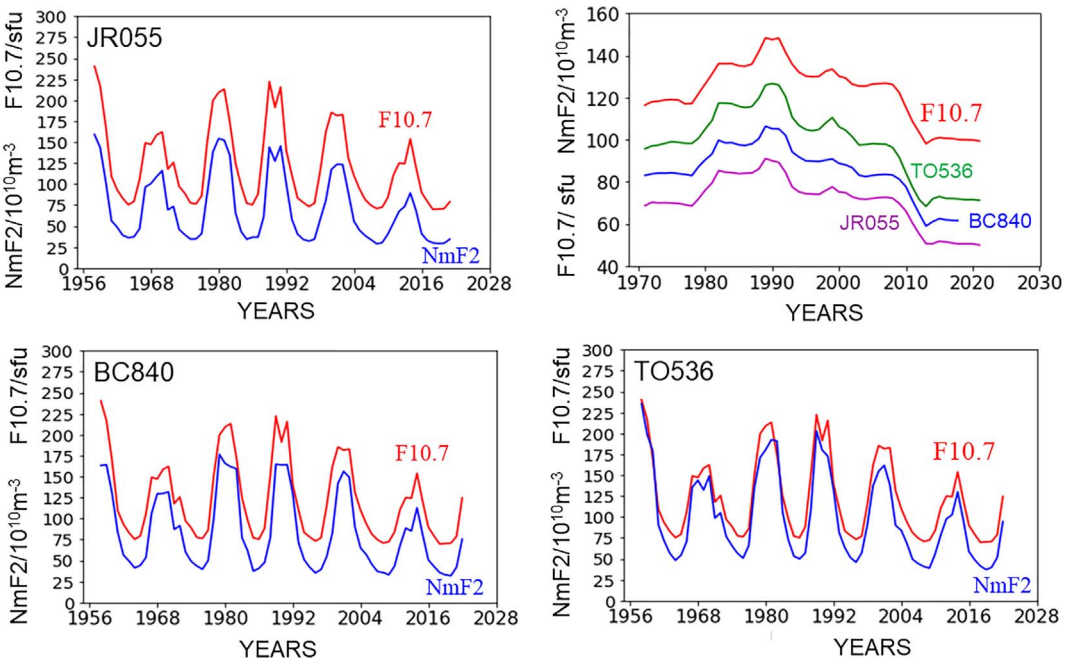

Figure 7. Long-term behavior of yearly averaged noontime NmF2 values for ionosonde stations JR055, BC840, and TO536 in comparison with the radio flux index F10.7. The upper right panel shows sliding previous 11 years' averages of F10.7 and NmF2 for all three ionosonde stations.

To further analyze the data in this respect, we suggest a new approach to better understand long-term trends and their physical background. Following Jakowski & Paasch (1984), we consider the rate of change of NmF2 and TEC at sunrise and sunset conditions (zenith angle 90°) to estimate the ionization rate and the loss rate of plasma, respectively. According to the basic knowledge of ionosphere physics, these quantities are related to atomic oxygen and molecular nitrogen concentrations, respectively. The physical background is approximated by the continuity equation describing the electron density rate of change in general, being aware that the ionospheric plasma is composed of different ion types and closely related to the thermosphere composition.

$$\frac{\partial n_e}{\partial t} = Q - L - \mathrm{div}(n_e \cdot v). \tag{6}$$

Here Q means the production term due to photoionization at daytime, L the loss term due to recombination, and the divergence term describes plasma loss and gain by transport processes. Ionization due to particle precipitation is ignored here because observations refer to mid-latitude stations. Specifying the production and loss terms in more detail, we can write:

$$\frac{\partial n_e}{\partial t} \approx \alpha \cdot I - \beta \cdot n_e - \mathrm{div}(n_e \cdot v) \tag{7}$$

where I indicate the ionizing radiation intensity, mostly EUV, n_e describes the electron density, α designates the production coefficient, β the loss coefficient, and v stands for the plasma velocity.

In a first approach, one can ignore the loss and divergence terms during sunrise hours because electron density values are still very low early in the morning. So, we get:

$$\frac{\partial n_e}{\partial t} \approx \alpha \cdot I \tag{8}$$

The production coefficient α is then estimated by:

$$\alpha \approx \frac{\partial n_e}{\partial t} / I. \tag{9}$$

The ionizing part of the solar irradiation can be approximated by the F10.7 index, i.e. assuming in the subsequent analysis $I \sim$ F10.7 one gets:

$$\alpha \sim \frac{1}{\mathrm{F10.7}} \frac{\partial n_e}{\partial t}. \tag{10}$$

Being aware that this approach is a very rough one it should be underlined that instead of deriving a physically correct absolute value for α we focus here on long-term relative changes in the production term. At heights of photo production maximum at around 180 km and above, the photoionization of atomic oxygen clearly dominates in creating ionospheric plasma. Following this approach, it is assumed that the α coefficient provides a proxy of atomic oxygen $\alpha \sim$ [O]. It is evident that the photoionization depends on the incidence angle of solar radiation. Focusing on long-term behavior, this dependence is ignored in the subsequent analysis justified by considering only one season with similar seasonal radiation conditions at each station. When considering sunset conditions, the photoionization can be ignored. However, due to the accumulated ionization at daytime, the electron density is usually much higher than during sunrise. Thus, coupling processes with the plasmasphere and related vertical plasma transport or wind-induced horizontal plasma transport may contribute via the divergence term to the

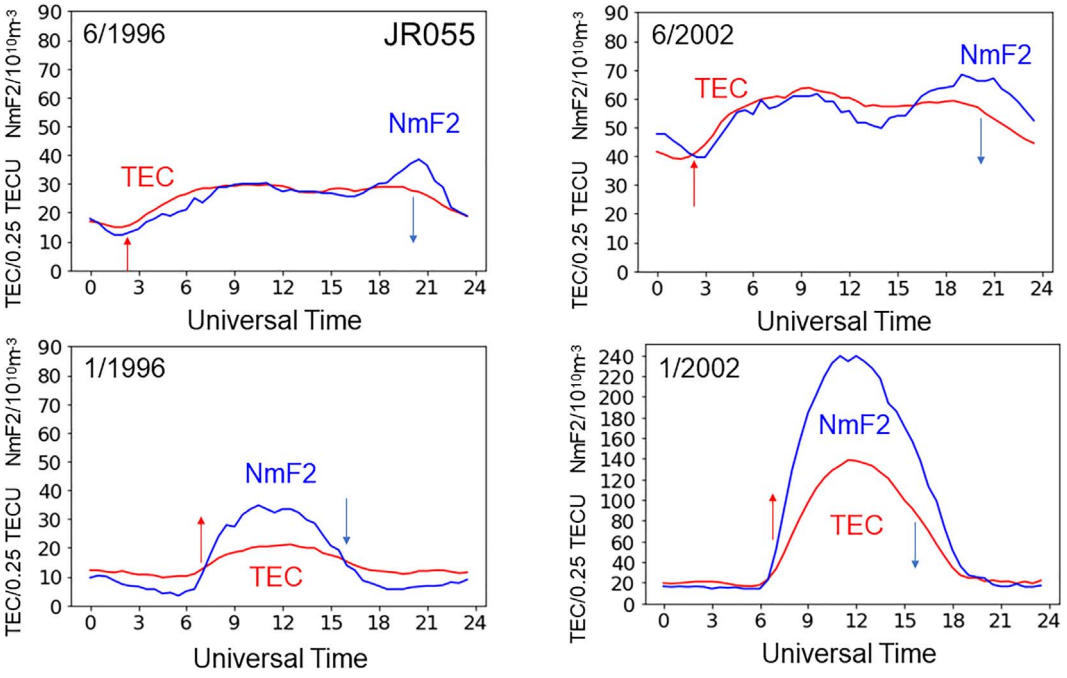

Figure 8. Diurnal variation of monthly medians of TEC and NmF2 over Juliusruh under low and high solar activity conditions in summer (June) and winter (January) in 1996 and 2002, respectively. Arrows mark sunrise (red) and sunset (blue).

balance of equation (6). The typical behavior of the peak electron density over Juliusruh during summer is shown in Figure 8 (upper panels) for low (1996) and high (2002) solar activity conditions.

Considering the increase of NmF2 around/after sunset hours under low as well as under high solar activity conditions, it is evident that plasma transport dominates over recombination processes at sunset hours in summer. In some cases, the diurnal maximum of the peak density NmF2 might even occur after sunset forming the Midlatitude Summer Nighttime Anomaly (MSNA) as seen in the upper panels of Figure 8 (e.g. Lin et al., 2010; Thampi et al., 2011). Contrary to this behavior in summer, a clear decrease of NmF2 is observed around sunset in winter indicating that recombination processes dominate as can be seen in the lower panels of Figure 8 characterizing winter conditions. Nevertheless, a return flux of plasma from the plasmasphere will also occur in winter. Under certain conditions, also at nighttime in winter strong coupling processes with the plasmasphere may increase the ionization forming the Nighttime Winter Anomaly (NWA) discovered by Jakowski et al. (1981, 1995, 2015) or cause nighttime enhancements (Jakowski et al., 1991) as observed in the Northern hemisphere at the American longitude sector and in the Southern hemisphere at the Asian longitude sector.

It is worth noting that the TEC does not show a strong difference between the summer and winter months because vertical plasma transport is a redistribution process of plasma inside the vertical integral of electron density with only secondary effects on TEC. Because vertical and/ or horizontal plasma transport is strong in summer, the months of April–October are principally excluded from estimating the recombination coefficient β according to:

$$\frac{\partial n_e}{\partial t} \approx -\beta \cdot n_e \tag{11}$$

providing an estimation of the β coefficient by:

$$\beta \sim -\frac{1}{n_e}\frac{\partial n_e}{\partial t}. \tag{12}$$

Since the β coefficient describes the loss term, i.e. the rate of recombination, it is assumed that β is a proxy of molecular neutral gas components, in particular of the N_2 density according to $\beta \sim [N_2]$. Since the recombination process requires both the conservation of energy and the conservation of momentum, a direct recombination of electrons with dominating O^+ ions is rather low. Thus, the recombination of electrons in the F2 layer is characterized by dissociative recombination where a third collision partner is available to fulfill both conservation laws easily. In this case, the recombination is proportional to n_e and the molecular constituents O_2 and N_2. Since the charge exchange of O^+ with N_2, followed by the recombination of electrons with NO^+ dominates, it is assumed that $\beta \sim [N_2]$.

Considering equations (10) and (12) and their relationships to neutral gas densities, by computing the ratio α/β one can estimate a proxy of the O/N_2 ratio that is crucial for understanding the variability of ionospheric ionization.

Instead of the electron density also the TEC can be considered in this way (Jakowski & Paasch 1984):

$$\int \frac{\partial n_e}{\partial t} \mathrm{d}h \approx I \cdot \int \alpha \, \mathrm{d}h - \int \beta \cdot n_e \mathrm{d}h - \int \mathrm{div}(n_e \cdot v) \mathrm{d}h. \tag{13}$$

Neglecting the transport term and applying the mean value theorem one gets:

$$\frac{\partial \mathrm{TEC}}{\partial t} \approx \bar{\alpha} \cdot I - \bar{\beta} \cdot \mathrm{TEC}. \qquad (14)$$

Thus, instead of α and β derived from peak electron density we consider now $\bar{\alpha}$ and $\bar{\beta}$ derived from TEC over the ionosonde stations selected. Both parameters are computed in analogy to equations (10) and (12) substituting n_e by TEC. Thus, instead of α and β we consider now $\bar{\alpha}$ and $\bar{\beta}$ derived from TEC over Juliusruh.

The production and loss coefficients α and β, computed from NmF2 and $\bar{\alpha}$ and $\bar{\beta}$ form TEC data over Juliusruh are shown in Figure 9 for the time period 1996–2022.

Monthly medians of production and loss coefficients presented in Figure 9 show a considerable seasonal as well as solar activity dependence. As indicated in Figure 8, NmF2 may even increase during sunset in summer $\left(\frac{\partial n_e}{\partial t} > 0 \text{ or } \beta^* > 0, \text{ i.e. } \beta < 0\right)$.

As indicated in the lower panel, $\bar{\beta}^*$ values for TEC are mostly below the zero line ($\beta > 0$) indicating a lower sensitivity of TEC against vertical plasma redistribution processes compared with NmF2 as expected. Nevertheless, to exclude the observed vertical plasma transport from further estimations of α and β (Fig. 8), we derive these parameters by averaging over the winter months of November, December, January, and February for subsequent analysis. So, one gets an α/β ratio that is representative only of winter conditions for NmF2 and TEC over the Juliusruh ionosonde station. It is worth mentioning that the estimated loss coefficient $\bar{\beta}$ of TEC is lower than for NmF2 nearly by a factor of two as seen in Figure 9. This indicates the rather stable contribution of the topside ionosphere and plasmasphere to the TEC that is practically not impacted by recombination.

For the period 1996–2022, the slopes of both α/β ratios are negative, for NmF2 −21.8% per decade and for TEC −22.2% per decade (Fig. 10 and Table 3). The loss coefficient slope in both cases is found to be positive, for NmF2 22.5% per decade and for TEC 16.6% per decade. The somewhat higher value of the percentage loss rate for NmF2 is probably related to the fact that the recombination mainly takes place in the bottom side ionosphere which is consistent with the higher absolute loss rate for NmF2 than for TEC. The stronger loss rate of NmF2 may indicate a long-term effect that might come from below.

Considering the impact of the plasmasphere, the loss terms derived from NmF2 data always provide a lower boundary, indicating that a plasmasphere-free ionosphere-related α/β ratio could even be stronger depending on related geophysical conditions. Nevertheless, the increase of β during recent solar cycles 22 and 23 is a strong indicator of a long-term growing loss rate, meaning that molecular constituents become more important in the electron density balance. Consequently, despite the less dynamic decrease of α compared with the F10.7 decrease, the α/β ratio for NmF2 as well as for TEC, decreases stronger than F10.7 over the entire period 1996–2022. Considering RMSE values of up to 30% for all three parameters, the discussed relationship of α, β and the α/β ratio with F10.7, is statistically not significant. Longer time series and a more detailed modeling approach can help to get deeper insight into the long-term behavior of these quantities.

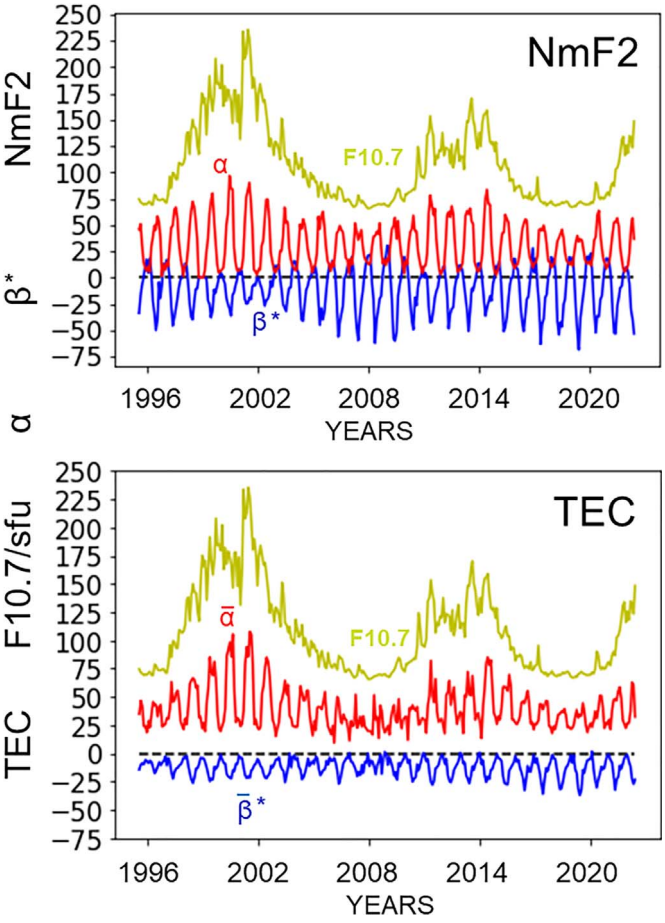

Figure 9. Production and loss coefficients α and $\beta^* = -\beta$, respectively, computed from peak electron density values over Juliusruh at corresponding local sunrise and sunset conditions in the time period 1996–2022 (upper panel). Units: α [$10^4 m^{-3} s^{-1}$/sfu], β [$2.5 \cdot 10^{-6}$ s^{-1}]. Production and loss coefficients $\bar{\alpha}$ and $\bar{\beta}^*$, respectively, computed from TEC values over Juliusruh during 1996–2022 (lower panel). To better separate production and loss coefficients, negative values of the loss coefficient $\bar{\beta}^* = -\bar{\beta}$ are plotted. Units: $\bar{\alpha}$ [$1.5 \cdot 10^{-4}$ mTECU s^{-1}/sfu], $\bar{\beta}$ [$2.5 \cdot 10^{-6}$ s^{-1}]

The fundamental question is whether the enhanced loss and decrease of the α/β ratio is only due to the solar activity change as could be argued also from studies covering time periods of less than two solar cycles (e.g. Zhang & Paxton 2011), or whether other long-term factors enhancing recombination processes in the ionosphere might play a role. Considering this challenge, we have analyzed long-term NmF2 data sets that have been generated at ionosonde stations Juliusruh, Boulder, and Kokubunji over the long observation period 1958–2022.

As Figure 11 shows, production and loss coefficients as well as their ratio are correlated with solar activity variation but with differences in the long-term behavior. Whereas the production term follows mostly the solar cycle behavior, the loss term behaves in the opposite way.

This is closely related to the cooling of the thermosphere and subsequent lowering of the peak density height and the equivalent slab thickness when solar activity decreases, as can

Table 3. Pearson correlation coefficients R and slopes of NmF2 related linear regression lines of α, β, and α/β for the period 1958–2022 (Fig. 12) and the shorter period 1996–2022 for TEC and NmF2 (Fig. 10). Furthermore, the corresponding Root Mean Square Errors (RMSE) and absolute as well as percentage values are given. Slope*, RMSE*: TEC units α [10^{-4} mTECU s^{-1} sfu^{-1}], β [10^{-6} s^{-1}], α/β [10^{1} mTECU sfu^{-1}].

Ionosonde station	Parameter unit	Production coefficient α [10^4 $m^{-3}s^{-1}sfu^{-1}$]/%	Loss coefficient β [10^{-6} s^{-1}]/%	Ratio α/β [10^8 $m^{-3}sfu^{-1}$]/%	Radio flux F10.7 [sfu]/%
JR055 NmF2 1958–2022	R	0.85	−0.78	0.89	–
	Slope	−0.78/−1.4	3.3/5.8	−5.4/−5.0	−4.4/−3.1
	RMSE	3.3/5.8	3.3/5.8	10.9/10.1	13.7/9.8
JR055 NmF2 1996–2022	R	0.90	−0.83	0.93	–
	Slope	−4.5/−7.5	14.0/22.5	−25.0/−21.8	−17.4/−12.4
	RMSE	10.4/17.3	14.0/23.1	26.0/22.8	38.5/27.6
JR055 TEC 1996–2022	R	0.93	0.16	0.86	–
	Slope*	−8.7/−16.2	8.5/16.6	−3.7/−22.2	−17.4/−12.9
	RMSE*	2.6/29.0	7.9/21.7	4.4/19.5	38.4/ 28.5
BC840 NmF2 1958–2022	R	0.36	−0.94	0.91	–
	Slope	−1.09/−1.7	3.7/4.5	−4.6/−4.9	−4.4/−3.1
	RMSE	1.8/2.8	7.8/9.6	11.5/ 12.3	13.7/9.8
TO536 NmF2 1958–2022	R	0.87	−0.87	0.89	–
	Slope	−1.5/−2.2	2.0/1.9	−3.9/−4.9	−4.4/−3.1
	RMSE	3.1/4.5	8.7/8.2	10.7/13.5	13.7/9.8

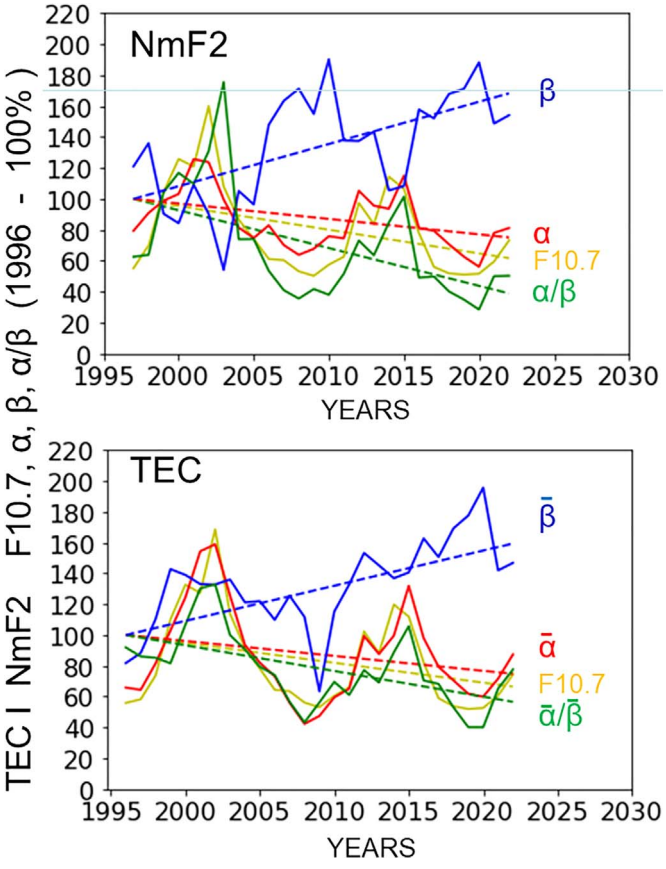

Figure 10. Production coefficient α and loss coefficient β derived from JR055 NmF2 data (upper panel) and TEC (lower panel) are shown in comparison with F10.7 and the α/β ratio over more than two solar cycles from 1996 to 2022. Regression lines and data are normalized to a value of 100 in 1996.

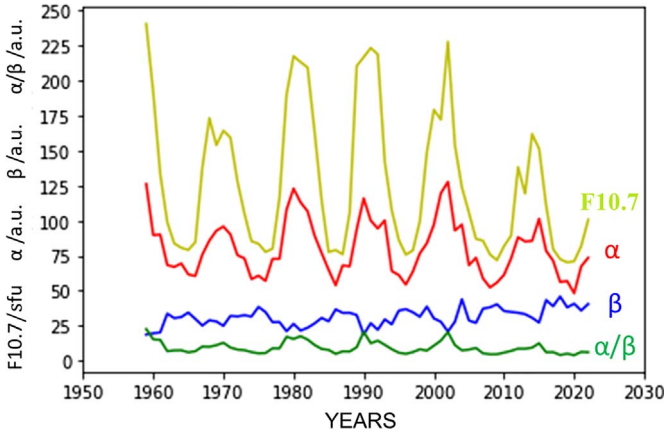

Figure 11. Production coefficient α, loss coefficient β and the ratio α/β computed from winter-time NmF2 data of the ionosonde station Juliusruh (JR055), in comparison with F10.7. Units: α [$6.67 \cdot 10^3$ $m^{-3}s^{-1}sfu^{-1}$], β [$2 \cdot 10^{-6}$ s^{-1}], α/β [10^9 $m^{-3}sfu^{-1}$].

be seen in Figures 5 and 3. Due to the lowering and contraction of the thermosphere/ionosphere system the impact of the molecular constituents goes up, i.e. recombination characterized by the loss coefficient β peaks during solar activity minima and increases with decreasing long-term solar activity in principal agreement with results obtained for the period 1996–2022 (Fig. 10).

To reduce the solar cycle impact, NmF2 data have been averaged over a full solar cycle period of 11 years. This is possible due to the availability of three data sets covering 65 years each.

Thus, Figure 12 shows the sliding average for production and loss coefficients α and β and their ratio α/β of the previous 11 years compared with F10.7 prepared in the same way. The overall increase of the loss coefficients and decreases in

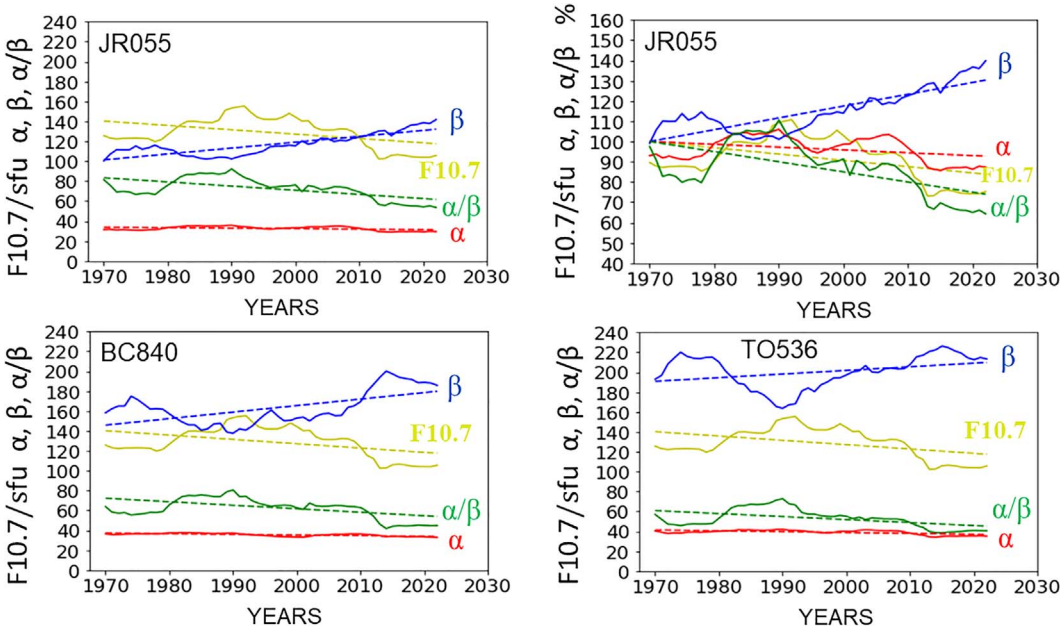

Figure 12. Previous 11 years sliding averages of production and loss coefficients and their ratio for selected stations in comparison with F10.7 including linear regression lines (dashed) over the period 1970–2022 (left and lower panel). Percentage decrease of the same parameters for Juliusruh (upper right panel) referring to 100% at 1970. Units: α [$1.67 \cdot 10^4$ m^{-3} s^{-1} sfu^{-1}], β [$5.6 \cdot 10^{-7}$ s^{-1}], α/β [$1.3 \cdot 10^8$ m^{-3} sfu^{-1}].

production and their ratio are indicated by linear regression lines. For optimal visualization all computations except for the upper right panel are made in the same way enabling a comparison of their absolute values at different stations. The upper right graphic shows for Juliusruh, as an example for the other two stations, percentage deviations for all parameters referring to the 100% level in the year 1970. The corresponding Pearson correlation coefficients, slopes of linear regression lines, and related RMSE values for all three stations are given in Table 3 including percentage deviations from reference values in 1970. Because the derived parameter values refer to the previous 11 years, any interpretation of the data must consider that related physical processes discussed in this chapter have been started at least 5–6 years earlier.

The long-term study reveals absolute changes per decade of about -0.8 up to $-1.5 \cdot 10^4$ $m^{-3}s^{-1}sfu^{-1}$ for the production coefficient α, an increase of the loss coefficient β of about 2.0 up to $3.7 \cdot 10^{-6}$ s^{-1} and -3.9 up to $-5.4 \cdot 10^4$ $m^{-3}s^{-1}sfu^{-1}$ for the α/β ratio. The corresponding percentage decreases per decade referenced to 100% in 1970 is -1.4 up to -2.2%, 1.9 up to 4.5%, and -4.9 up to -5.0%, respectively. The percentage long-term decrease per decade of the α/β ratio is with about 5% very similar at all stations. The RMSE values are up to a factor of about 4 higher than the slope values thus indicating that the derived values are not always statistically significant. However, it should be noted that all three ionosonde stations show a very similar behavior thus enhancing the reliability of the estimates.

Whereas the normalized analysis as shown in the upper right panel of Figure 12 provides percentage decrease values of analyzed parameters for the three stations (see Table 3), the other plots enable a comparison of absolute parameters as a function of the geographic latitude.

A comparison of stations provides good insight into the basics of underlying ionospheric physics.

The absolute decrease values of α are somewhat stronger over Kokubunji than over Juliusruh due to a lower latitude i.e. a lower incidence angle of solar radiation. Contrary to the slight differences in percentage decreases of α at ionosonde stations, the absolute values of the loss coefficient β go up considerably towards lower latitudes as a comparison of the β plots from different stations clearly shows in Figure 12, nearly by a factor of two when comparing Kokubunji and Juliusruh. This finding can be explained mainly by stronger solar incidence at lower latitudes and associated higher temperatures in the thermosphere, in particular also greater scale heights of molecular constituents like N_2 and O_2. Also, the production coefficient α that is a proxy of atomic oxygen, changes enormously after 1996 indicated by a decrease of 7.5% per decade at Juliusruh for the 1996–2022 period. The general increase of the loss coefficient β and the decrease of the production term α lead to a long-term percentage decrease for the α/β (~O/N_2) ratio of 21.8%.

3.4 Linear models of NmF2 and foF2 as a function of the solar radio flux index F10.7

Considering the rather strong decrease of foF2 and the corresponding peak electron density NmF2 in the period 1996–2022 (cf. Fig. 3 and Table 2), we study their relationship with F10.7 in more detail using the NmF2 values derived from foF2 observations at the three selected ionosonde stations. The 11-years averages of NmF2 in Figures 7 and 13 in the upper right panels show at first view a high correlation with F10.7 as expected.

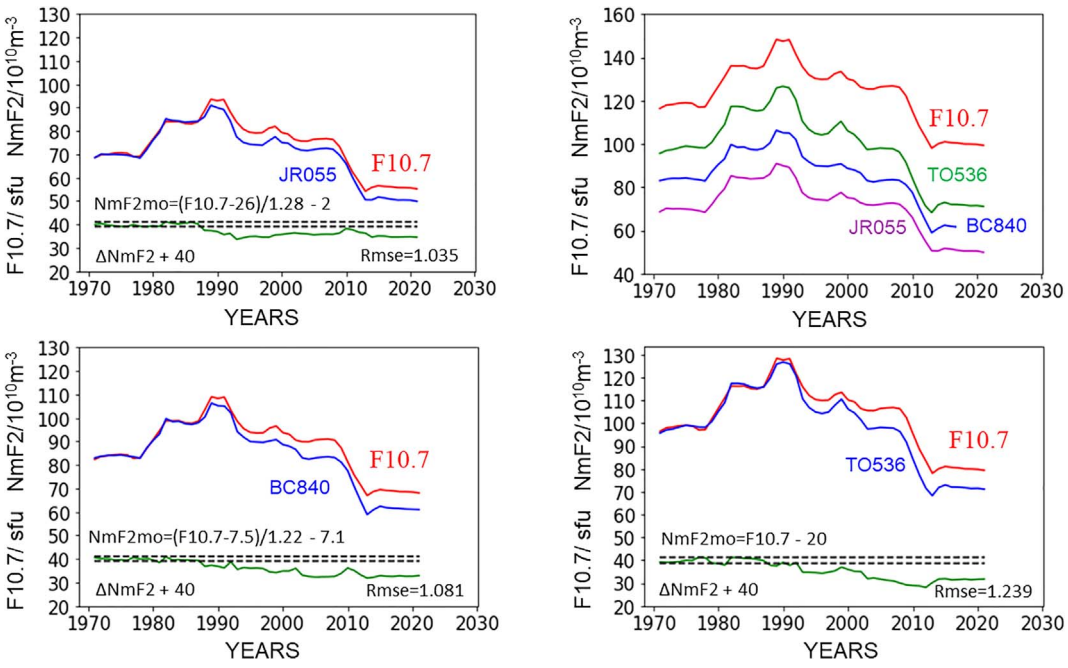

Figure 13. Previous 11 years sliding averages of F10.7 and modelled NmF2 noontime (13–14 LT) data over Juliusruh, Boulder, and Kokubunji at left and lower panels. The upper right panel shows absolute sliding previous 11 years' averages of F10.7 and NmF2 at all three ionosonde stations as already shown in Figure 7. Dashed lines indicate the RMSE range of linear NmF2 models.

To study the long-term trend in more detail we follow a linear modeling approach of foF2 and NmF2 with solar activity parameters utilized in many publications (e.g. Laštovička et al., 2017; Perrone et al., 2017; Laštovička & Jelínek, 2019, Sivakandan et al., 2023). To check the consistency of the long-term behavior of foF2 and NmF2 we have developed linear models for all three stations both for foF2 and NmF2. As Figures 13 and 14 show, a linear relationship of 11-years averaged values for foF2 and NmF2 with F10.7 worked very well until about 1990. The corresponding RMSE values as seen in Table 4 are very low at all three stations. Nevertheless, due to the nonlinear relationship between NmF2 and foF2 as given by equation (2), the linear fit may not be a correct approximation for at least one of these variables. Probably due to this, we see a difference between both linear approaches in Figures 12 and 13 that require a more detailed analysis. A remarkable difference is indicated by different onset times of the deviation from the linear approach. Thus, the models (blue curves) start to deviate from F10.7 (red curve) between 1980 and 1990 for NmF2 and shortly after 1990 for foF2. As the corresponding deviation plots at the bottom of the panels (zero line shifted to 40) show, the deviation exceeds the RMSE range of the models clearly. As in particular shown in Figure 14, the difference is growing with the years.

As already previously discussed, the α/β ratio shows a stronger decrease in the period after 1996 than before (Table 3). More detailed studies including numerical modelling can check the relationship between the α/β ratio and the deviation of the linear model from F10.7 after 1990.

It is worth mentioning that the clear deviation from rather good linear models valid up to about 1985–1990 appears at all three ionosonde stations showing an enhancement towards lower latitudes.

It is interesting to note that Danilov & Konstantinova (2013) have already addressed a different behavior of the foF2 between the period 1958–1979 and 1998–2010. They concluded that the negative trends in the critical frequencies of the F2 layer after 1990 are substantially higher than the ones derived for earlier periods. This finding was studied later in more detail by Danilov (2017) considering the period 1958–1980 as "etalon" period. He concluded that in the process of cooling and contraction of the thermosphere the atomic oxygen concentration decreases. Perrone et al. (2017) also assumed a decrease in atomic oxygen but mentioned an increase in the O/N_2 ratio after 1990. Our findings agree with the conclusion of an enhanced decrease of atomic oxygen but underline also an increase of the loss term β ($\sim N_2$) after 1980–1990 associated with an enhanced decrease of the α/β ratio ($\sim O/N_2$) for the latitude range 35–55 °N approximately covered by the three ionosonde stations considered in this paper. The divergence between F10.7 and modeled foF2 and NmF2 after 1990, being aware that the related physical processes lie in the 1980–1990 decade, may have different reasons. First, one should consider, that the relationship between F10.7 and NmF2 or foF2 is not purely linear. Furthermore, the solar radiation spectrum between the 10.7 cm ratio flux and ionizing EUV components could have been changed (e.g. Tapping & Valdés, 2011). Solomon et al. (2010) reported a strong decrease in solar EUV radiation between 1996 and 2008. Other options are changes in geomagnetic activity (Mikhailov & Marin, 2001; Cnossen & Franzke, 2014), of dynamic coupling processes from below e.g. gravity waves (Oliver et al., 2013). Considering the location of selected ionosonde stations, long-term changes in

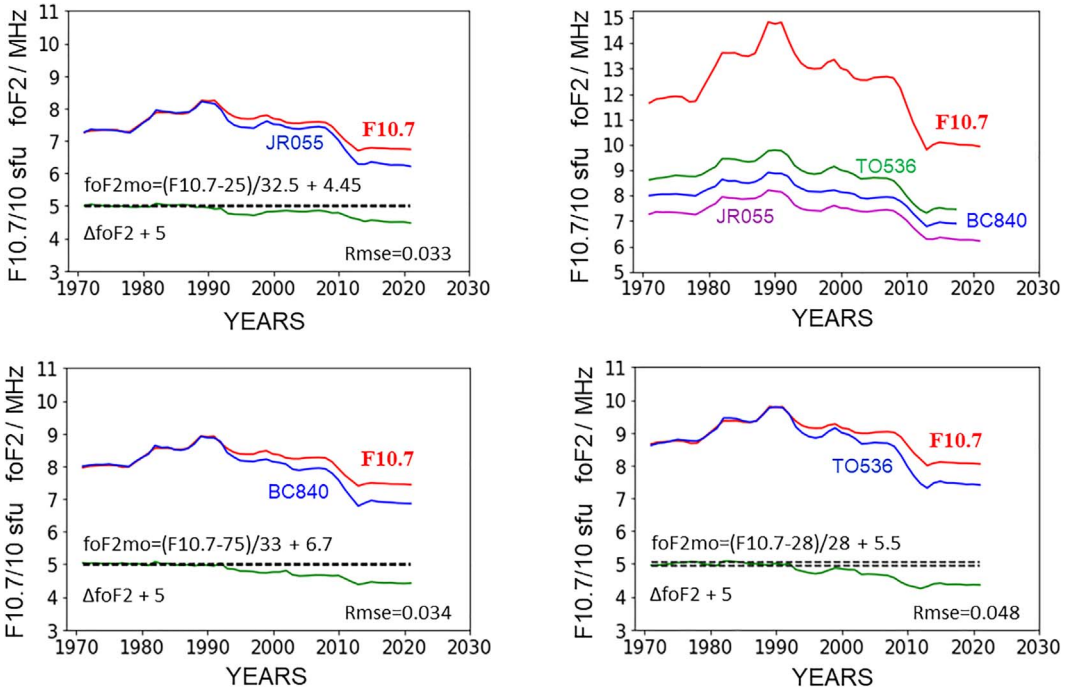

Figure 14. Previous 11 years sliding averages of F10.7 and modelled foF2 noontime (13–14 LT) data over Juliusruh, Boulder, and Kokubunji at left and lower panels. The upper right panel shows running previous 11 years' averages of F10.7 and foF2 at all three ionosonde stations. Dashed lines indicate the RMSE range of linear foF2 models.

Table 4. Pearson correlation coefficients R and linear models of NmF2 and foF2 from F10.7 including RMSE values using previous 11 years averaged peak density and critical frequency data covering the period 1958–1990 (Figs. 13 and 14).

Ionosonde station	Variable	Unit	Linear function f $f = f(\text{F10.7})$	Correlation R	RMSE
Juliusruh JR055	NmF2	10^{10} m^{-3}	NmF2 = 0.78 × F10.7 − 20.31	0.98	1.035
	foF2	MHz	foF2 = 0.031 × F10.7 + 3.68	0.97	0.033
Boulder BC840	NmF2	10^{10} m^{-3}	NmF2 = 0.82 × F10.7 − 13.25	0.98	1.081
	foF2	MHz	foF2 = 0.03 × F10.7 + 4.43	0.97	0.034
Kokubunji TO536	NmF2	10^{10} m^{-3}	NmF2 = F10.7 − 20.0	0.98	1.239
	foF2	MHz	foF2 = 0.036 × F10.7 + 4.5	0.97	0.048

the geomagnetic field should be relatively small and any effects of these on NmF2 or foF2 are expected to be negligible (cf. Cnossen & Richmond, 2013).

An intensively discussed option refers to upward propagating trace gases such as CO_2, CH_4, or Ozone in the atmosphere that could modify the chemistry and physics of the MIT system (e.g. Qian et al., 2006, 2009; Solomon et al., 2015). The latter has been a topic of numerous papers investigating long-term trends in the MIT system. Most of the papers refer to the analysis of the F2 layer critical frequency foF2 (e.g. Bremer, 1992; Mikhailov & Marin, 2001; Laštovička et al., 2006; Bremer et al., 2012; Mielich & Bremer, 2013; Cnossen & Franzke, 2014; Danilov, 2017; Perrone et al., 2017; Laštovička, 2022; Sivakandan et al., 2023).

Considering the broad spectrum of impact factors, more detailed studies are needed to get a reliable explanation of the divergence between F10.7 and NmF2 after 1990 and associated scientific questions. We believe that the analysis of production and loss coefficients including their ratio at more ionosonde stations can contribute to improving our understanding long-term effects in ionospheric behavior.

4 Summary and conclusions

Peak electron density data derived from long-term vertical sounding measurements performed at the ionosonde stations Juliusruh (JR055), Boulder (BC840), and Kokubunji (TO536) during 1958–2022 have been utilized to estimate the long-term behavior of daytime ionospheric F2 layer ionization in relation to the solar F10.7 cm radio flux. In parallel, GNSS-based vertical TEC data over the ionosonde stations have been used to derive the equivalent slab thickness τ for estimating the long-term behavior starting in 1996, half a year after GPS became

operational. In the period 1996–2022, the noontime equivalent slab thickness values over Juliusruh follow the negative tendency of F10.7 and decrease by about 25 km per decade. The F2 layer peak height hmF2 decreases by about 12 km/decade. It has been indicated that τ can estimate the neutral gas temperature T_n around noon. Assuming a linear relationship between the equivalent slab thickness around noon and the neutral gas scale height the neutral gas temperature follows the solar cycle activity like the equivalent slab thickness. The neutral gas temperature T_n has been estimated to decrease by about 100 K per decade over Juliusruh at a height of about 350–400 km in the period 1996–2022 covering a temperature range between about 800 and 1300 K. Considering reported thermospheric cooling of up to about 10 K per decade over 33 years (e.g. Ogawa et al., 2014), the equivalent slab thickness would change by approximately 1–3 km. Considering the high variability of the equivalent slab thickness, it is concluded that monitoring anthropogenic-induced cooling of the thermosphere based on equivalent slab thickness data is extremely difficult over only two solar cycles. To get additional information regarding the production and loss processes in the ionosphere, a new method has been developed to estimate their long-term behavior from ionosonde data. Thus, the production coefficient α and the loss coefficient β, enabling computing the α/β ratio, have been estimated for winter months near local sunrise and sunset, respectively. These parameters are assumed to provide proxies for the atomic oxygen concentration ($\alpha \sim [O]$) and the concentration of molecular constituents, mainly nitrogen ($\beta \sim [N_2]$). Knowledge of both parameters allows estimating the O/N_2 ratio which is crucial for understanding the behavior of the ionosphere. It has been found that the O/N_2 ratio follows mostly the variation of the solar activity level characterized by the 10.7 cm radio flux. The NmF2-related estimation of the production coefficient α and the ratio α/β reveal a linear decrease of about 2–5% per decade over the period 1958–2022. The loss coefficient β goes up in the same order at the three ionosonde stations. Although the RMSE values are rather high for this rough approach the long-term change is confirmed at all three ionosonde stations. More detailed studies including numerical modeling can get deeper insight into the role of the long-term development of production and loss coefficients and their ratio, in particular also to better understand the long-term behavior of NmF2 and/or foF2.

In parallel with the F10.7 decrease of about 20 sfu per decade in the period 1996–2022, the noontime (12–14 LT) peak electron density decreases by about $14 \cdot 10^{10}$ m^{-3} over Juliusruh and the critical F2 layer frequency by about 0.7 MHz per decade. The corresponding values for the other stations differ somewhat due to shorter observation periods. It is concluded that the estimation of reliable long-term trends in the MIT system requires more than two solar cycles. All parameters, except the equivalent slab thickness τ, are highly correlated with F10.7 expressed by correlation coefficients ranging from 0.94 to 0.99. The long-term analysis covering 65 years of foF2 observations reveals a high correlation with F10.7 up to 1990 for 11 years averaged values of foF2 and NmF2. However, there are strong indications that the relationship between foF2 and NmF2 with F10.7 is changing after the 1980–1990 decade indicated by clear deviations of the linear models from the 11-year averaged F10.7 variation. This changed behavior might have different reasons such as changes in the solar spectrum, geomagnetic activity, or coupling processes from below including thermospheric composition changes due to the enhanced density of greenhouse gases.

More detailed studies including numerical modeling are needed to better understand the contribution of different MIT processes to the decoupling of the linear model of the daytime F2 layer electron density from the solar radio flux index F10.7.

Acknowledgements

The authors thank the sponsors and operators of the ionosonde stations Juliusruh, Boulder, and Kokubunji for maintaining vertical sounding over many years and making the data available. We thank also the Space Environment Laboratory, Applied Electromagnetic Research Institute, National Institute of Information and Communications Technology, Japan (https://wdc.nict.go.jp/IONO/HP2009/ISDJ/index-E.html.), the UK Solar System Data Centre, STFC Rutherford Appleton Laboratory, United Kingdom (https://www.ukssdc.ac.uk/cgi-bin/wdcc1/secure/iono_data.pl) and the Global Ionosphere Radio Observatory (GIRO), United States (https://giro.uml.edu/didbportal/didb-web-portal/) for providing ionosonde data via internet access. The authors would like to acknowledge also the support of the University of Bern contributing to the IGS by providing CODE TEC data to the Crustal Dynamics Data Information System (CDDIS) for free access via the internet (https://cddis.nasa.gov/archive/gnss/data/). Furthermore, the authors thank the NOAA National Geophysical Data Center for providing F10.7 solar radio flux index data (https://www.ngdc.noaa.gov/stp/space-weather/solar-data/solar-features/solarradio/noontimeflux/penticton/penticton_absolute/listings/listing_drao_noontime-flux-absolute_monthly.txt). The editor thanks Stephan Buchert and an anonymous reviewer for their assistance in evaluating this paper.

References

Bremer J. 1992. Ionospheric trends in mid-latitudes as a possible indicator of the atmospheric greenhouse effect. *J Atmos Terr Phys* **54**: 1505–1511. https://doi.org/10.1016/0021-9169(92)90157-G.

Bremer J, Damboldt T, Mielich J, Suessmann P. 2012. Comparing long-term trends in the ionospheric F2-region with two different methods. *J Atmos Terr Phys* **77**: 174–185. https://doi.org/doi.org/10.1016/j.jastp.2011.12.017.

Cai Y, Yue X, Wang W, Zhang S, Liu L, Liu H, Wan W. 2019. Long-term trend of topside ionospheric electron density derived from DMSP data during 1995–2017. *J Geophys Res Space Phys* **124**: 10708–10727. https://doi.org/10.1029/2019JA027522

Cnossen I, Franzke C. 2014. The role of the Sun in long-term change in the F2 peak ionosphere: new insights from EEMD and numerical modelling. *J Geophys Res Space Phys* **119**: 8610–8623. https://doi.org/10.1002/2014JA020048.

Cnossen I, Richmond AD. 2008. Modeling the effects of changes in the Earth's magnetic field from 1957 to 1997 on the ionospheric hmF2 and fof2 parameters. *J Atmos Sol Terr Phys* **70**: 1512–1524. https://doi.org/10.1016/j.jastp.2008.05.003.

Cnossen I, Richmond AD. 2013. Changes in the Earth's magnetic field over the past century: effects on the ionosphere-thermosphere system and solar quiet (Sq) magnetic variation. *J Geophys Res Space Phys* **118**: 849–858. https://doi.org/10.1029/2012JA018447.

Danilov AD, Konstantinova AV. 2013. Behavior of the ionospheric F2 layer parameters at the boundary of centuries (2013) Critical frequency. *Geomagn Aeron* **53**: 345–355. https://doi.org/10.1134/S0016793213030043.

Danilov A. 2017. New results in studying foF2 trends. *J Atmos Sol Terr Phys* **163**: 103–113. https://doi.org/10.1016/j.jastp.2017.04.002.

Elias AG, Zossi de Artigas M, De Haro Barbas BF. 2010. Trends in the solar quiet geomagnetic field variation linked to the Earth's magnetic field secular variation and increasing concentrations of greenhouse gases. *J Geophys Res* **115**: A08316. https://doi.org/10.1029/2009JA015136.

Emmert JT, Lean JL, Picone JM. 2010. Record-low thermospheric density during the 2008 solar minimum. *Geophys Res Lett* **37**: L12102. https://doi.org/10.1029/2010/GL043671.

Emmert JT, Mannucci AJ, McDonald SE, Vergados P. 2017. Attribution of interminimum changes in global and hemispheric total electron content. *J Geophys Res Space Phys* **122**: 2424–2439. https://doi.org/10.1002/2016JA023680.

Hall C, Rypdal K, Rypdal M. 2011. The E region at 69°N, 19°E: trends, significances, and detectability. *J Geophys Res* **116**. https://doi.org/10.1029/2011JA016431

Jakowski N, Bettac HD, Lazo B, Lois L. 1981. Seasonal variations of the columnar electron content of the ionosphere observed in Havana from July 1974 to April 1975. *J Atmos Sol Terr Phys* **43**: 7–11. https://doi.org/doi.org/10.1016/0021-9169(81)90003-9.

Jakowski N, Paasch E. 1984. Report on the observations of the total electron content of the ionosphere in Neustrelitz/GDR from 1976 to 1980. *Ann Geophys* **2**: 501–504.

Jakowski N, Jungstand A, Lois L, Lazo B. 1991. Night-time enhancements of the F2-layer ionization over Havana. *J Atmos Terr Phys* **53**: 1131–1138. https://doi.org/10.1016/0021-9169(91)90062-C.

Jakowski N, Förster M. 1995. About the nature of the Night-time Winter Anomaly effect (NWA) in the F-region of the ionosphere. *Planet Space Sci* **43**: 603–612. https://doi.org/10.1016/0032-0633(94)00115-8.

Jakowski N, Hoque MM, Kriegel M, Patidar V. 2015. The persistence of the NWA effect during the low solar activity period 2007–2009. *J Geophys Res Space Phys* **120**: 9148–9160. https://doi.org/10.1002/2015JA021600.

Jakowski N. 1996. TEC monitoring by using satellite positioning systems. In: *Modern ionospheric science*. Kohl H, Ruester R, Schlegel K, (Eds.) EGS, Katlenburg-Lindau, ProduServ GmbH Verlagsservice, Berlin. pp. 371–390. ISBN 3-9804862-1-4.

Jakowski N, Mayer C, Missling KD, Becker C, Borries C, Daedelow H, Dubey S, Noack T, Tegler M, Wilken V. 2008. Space weather application center ionosphere – new capabilities for GNSS users. In: Proceedings of the Fifth European Space Weather Week, Brussels, Belgium, 17–21 November.

Jakowski N, Mayer C, Hoque MM, Wilken V. 2011. Total electron content models and their use in ionosphere monitoring. *Radio Sci.* **46**: RS0D18. https://doi.org/10.1029/2010RS004620.

Jakowski N, Hoque MM, Mielich J, Hall C. 2017. Equivalent slab thickness of the ionosphere over Europe as an indicator of long-term temperature changes in the thermosphere. *J Atmos Sol Terr Phys* **163**, **2017**: 91–102. https://doi.org/10.1016/j.jastp.2017.04.008.

Jakowski N, Hoque MM. 2018. A new electron density model of the plasmasphere for operational applications and services. *J. Space Weather Space Clim* **8**: A16. https://doi.org/10.1051/swsc/2018002.

Laštovička J, Mikhailov AV, Ulich T, Danilov AD. 2006. Long-term trends in foF2: A comparison of various methods. *J Atmos Sol Terr Phys* **68**: 1854–1870. https://doi.org/10.1016/j.jastp.2006.02.009.

Laštovička J, Solomon SC, Qian L. 2012. Trends in the neutral and ionized upper atmosphere. *Space Sci Rev* **168**: 113–145. https://doi.org/10.1007/s11214-011-9799-3.

Laštovička J, Urbar J, Kozubek M. 2017. Long-term trends in the total electron content. *Geophys Res Lett* **44**: 8168–8172. https://doi.org/10.1002/2017GL075063.

Laštovička J, Jelínek Š. 2019. Problems in calculating long-term trends in the upper atmosphere, Journal of Atmospheric. *J Atmos Sol Terr Phys* **189**: 80–86. https://doi.org/10.1016/j.jastp.2019.04.011.

Laštovička J. 2022. Long-term changes in ionospheric climate in terms of foF2. *Atmosphere* **13**: 110. https://doi.org/10.3390/atmos13010110.

Lean JL, Meier RR, Picone JM, Sassi F, Emmert JT, Richards PG. 2016. Ionospheric total electron content: Spatial patterns of variability. *J Geophys Res Space Phys* **121**: 10367–10402. https://doi.org/10.1002/2016JA023210.

Lin CH, Liu CH, Liu JY, Chen CH, Burns AG, Wang W. 2010. Midlatitude summer nighttime anomaly of the ionospheric electron density observed by FORMOSAT-3/COSMIC. *J Geophys Res* **115**: A03308. https://doi.org/10.1029/2009JA014084.

Mielich J, Bremer J. 2013. Long-term trends in the ionospheric F2 region with different solar activity indices. *Ann Geophys* **31**: 291–303. https://doi.org/10.5194/angeo-31-291-2013.

Mikhailov AV, Marin D. 2001. An interpretation of the foF2 and hmF2 long-term trends in the framework of the geomagnetic control concept. *Ann Geophys* **19**: 733–748. https://doi.org/10.5194/angeo-19-733-2001.

Noll CE. 2010. The crustal dynamics data information system: a resource to support scientific analysis using space geodesy. *Adv Space Res* **45(12)**: 1421–1440. https://doi.org/10.1016/j.asr.2010.01.018.

Ogawa Y, Motoba T, Buchert SC, Häggström I, Nozawa S. 2014. Upper atmosphere cooling over the past 33 years. *Geophys Res Lett* **41**: 5629–5635. https://doi.org/10.1002/2014GL060591.

Oliver WL, Zhang SR, Goncharenko LP. 2013. Is thermospheric global cooling caused by gravity waves? *J Geophys Res Space Phys* **118**: 3898–3908. https://doi.org/10.1002/jgra.50370

Perrone L, Mikhailov A, Cesaroni C, Alfonsi L, De Santis A, Pezzopane M, Scotto C. 2017. Long-term variations of the upper atmosphere parameters on Rome ionosonde observations and their interpretation. *J. Space Weather Space Clim.* **7**: A21. https://doi.org/10.1051/swsc/2017021.

Qian L, Roble RG, Solomon SC, Kane TJ. 2006. Calculated and observed climate change in the thermosphere, and a prediction for solar cycle 24. *Geophys Res Lett* **33**: L23705. https://doi.org/10.1029/2006GL027185.

Qian L, Burns AG, Solomon SC, Roble RG. 2009. The effect of carbon dioxide cooling on trends in the F2-layer ionosphere. *J Atmos Sol Terr Phys* **71**: 1592–1601. https://doi.org/10.1016/j.jastp.2009.03.006.

Reinisch BW, Galkin IA. 2011. Global ionospheric radio observatory (GIRO). *Earth Planet Space* **63**: 377–381. https://doi.org/10.5047/eps.2011.03.001.

Rishbeth H. 1990. A greenhouse effect in the ionosphere? *Planet Space Sci* **38**: 945–948. https://doi.org/10.1016/0032-0633(90)90061-T.

Rishbeth H. 1997. Long-term changes in the ionosphere. *Adv Space Res* **20**: 2149–2155. https://doi.org/10.1016/S0273-1177(97)00607-8.

Roble RG, Dickinson RE. 1989. How will changes in carbon dioxide and methane modify the mean structure of the mesosphere and thermosphere? *Geophys Res Lett* **16**: 1441–1444. https://doi.org/10.1029/GL016i012p01441.

Shimazaki T. 1955. World-wide daily variations in the height of the maximum electron density in the ionospheric F2 layer. *J Radio Res Labs Japan* **2**: 85–97.

Schaer S, Beutler G, Rothacher M. 1998. Mapping and Predicting the Ionosphere. In: *Proceedings of the 1998 IGS Analysis Center Workshop, Darmstadt, February 9–11*, Dow JM, Kouba J, Springer T, (Eds.), ESA/ESOC, Darmstadt. pp. 307–318.

Sivakandan M, Mielich J, Renkwitz T, Chau JL, Jaen J, Laštovička J. 2023. Long-term variations and residual trends in the E, F, and sporadic E (Es) layer over Juliusruh, Europe. *J Geophys Res Space Phys* **128**: e2022JA031097. https://doi.org/10.1029/2022JA031097.

Solomon SC, Woods TN, Didkovsky LV, Emmert JT, Qian L. 2010. Anomalously low solar extreme-ultraviolet irradiance and thermospheric density during solar minimum. *Geophys Res Lett* **37**: L16103. https://doi.org/10.1029/2010GL044468.

Solomon SC, Qian L, Roble RG. 2015. New 3-D simulations of climate change in the thermosphere. *J Geophys Res Space Phys* **120**: 2183–2193. https://doi.org/10.1002/2014JA020886.

Tapping KF, Valdés JJ. 2011. Did the sun change its behaviour during the decline of cycle 23 and into cycle 24? *Solar Phys* **272**: 337–350. https://doi.org/10.1007/s11207-011-9827-1.

Thampi SV, Balan N, Lin C, Liu H, Yamamoto M. 2011. Mid-latitude Summer Nighttime Anomaly (MSNA) – observations and model simulations. *Ann Geophys* **29**: 157–165. https://doi.org/10.5194/angeo-29-157-2011.

Titheridge JE. 1973. The slab thickness of the mid-latitude ionosphere. *Planet Space Sci* **21(10)**: 1775–1793. https://doi.org/10.1016/0032-0633(73)90168-2.

Torr DG, Torr MR, Richards PG. 1980. Causes of the F region winter anomaly. *Geophys Res Lett* **7**: 301–304. https://doi.org/10.1029/GL007i005p00301.

Ulich T, Clilverd MA, Rishbeth H. 2003. Determining long-term change in the ionosphere. *Eos Trans* **84(52)**: 581–585. https://doi.org/10.1029/2003EO520002.

Wintoft P. 2011. The variability of solar EUV: a multiscale comparison between sunspot number, 10.7cm flux, LASP MgII index, and SOHO/SEM EUV flux. *J Atmos Sol Terr Phys* **73**: 1708–1714. https://doi.org/10.1016/j.jastp.2011.03.009.

Zhang Y, Paxton LX. 2011. Long-term variation in the thermosphere: TIMED/GUVI observations. *J Geophys Res* **116**: A00H02. https://doi.org/10.1029/2010JA016337.

Zhang Y, Wu Z, Feng J, Xu T, Deng Z, Ou M, Xiong W, Zhen W. 2021. Statistical study of ionospheric equivalent slab thickness at Guam magnetic equatorial location. *Remote Sens* **13**: 5175. https://doi.org/10.3390/rs13245175.

Cite this article as: Jakowski N, Hoque MM & Mielich J. 2024. Long-term relationships of ionospheric electron density with solar activity. *J. Space Weather Space Clim.* **14**, 24. https://doi.org/10.1051/swsc/2024023.